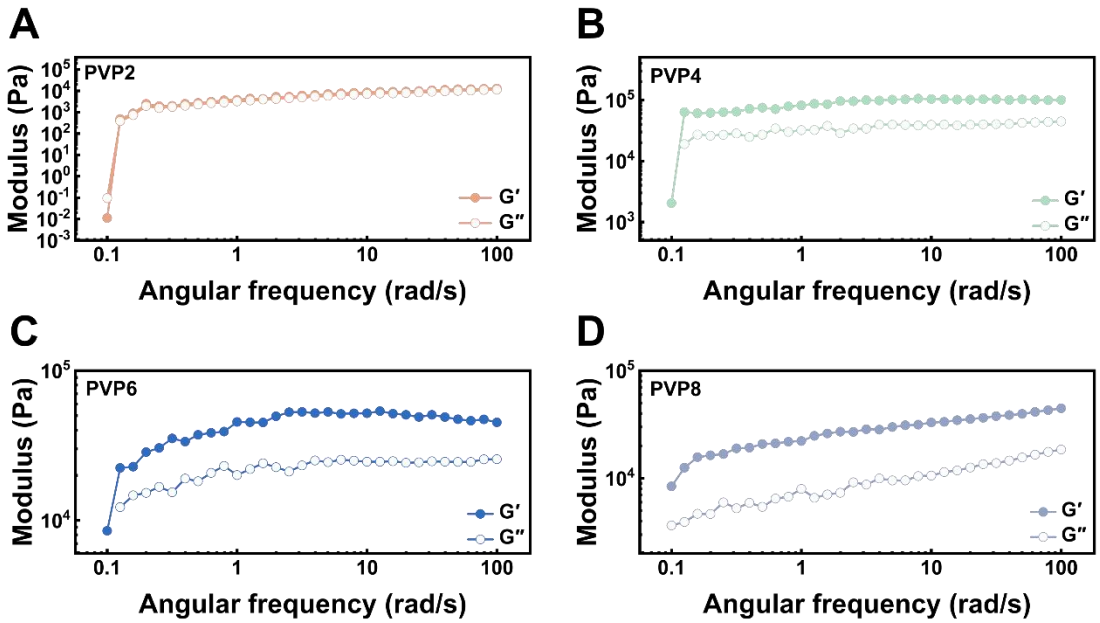
Supplementary Materials

Flexible and oxidation-resistant graphene@SiC nanofiber fabrics

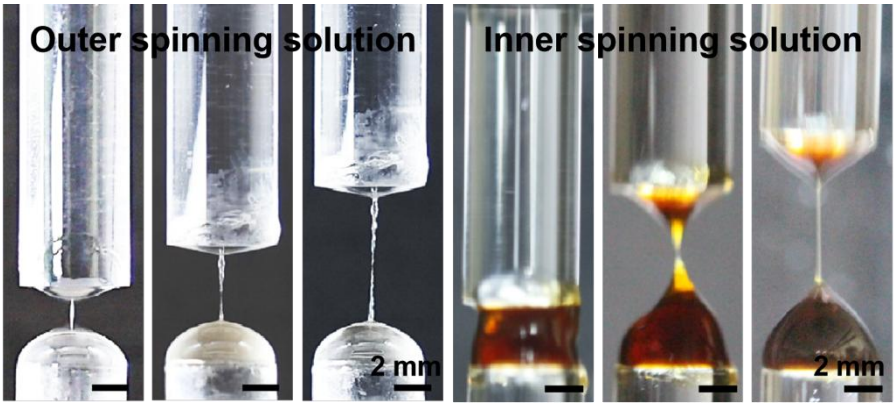
Shuai Lu[1,2,3], Zhanpo Han[2,4], Chang Shu[2], Zhiyao Zheng[2], Zhijie Zhou[2,5], Yifan Yao[2,6], Yi Han[7,*], Xinxin Jin[1,*], Zheng Li[2,*]

[1]Shao Xing Institute of Technology, School of Pharmacy and Health Sciences, Shaoxing Institute of Technology, Shaoxing 312000, Zhejiang, China.
[2]ZJU-Hangzhou Global Scientific and Technological Innovation Center, Key Laboratory for Biomedical Engineering of Education Ministry, Zhejiang Key Laboratory of Intelligent Sensing Technology and Advanced Medical Instrument, College of Biomedical Engineering & Instrument Science, Zhejiang University, Hangzhou 310027, Zhejiang, China.
[3]School of Materials Science and Chemical Engineering, Harbin University of Science and Technology, Harbin 150040, Heilongjiang, China.
[4]National Key Laboratory of Science and Technology on Advanced Composites in Special Environments, Harbin Institute of Technology, Harbin 150080, Heilongjiang, China.
[5]State Key Laboratory of Flexible Electronics (LoFE) & Jiangsu Key Laboratory of Smart Biomaterials and Theranostic Technology, Institute of Advanced Materials (IAM), Nanjing University of Posts and Telecommunications, Nanjing 210023, Jiangsu, China.
[6]College of Integrated Circuits, Zhejiang University, Hangzhou 311200, Zhejiang, China.
[7]Hangzhou Gaoxi Technology Co., Ltd, Hangzhou 311113, Zhejiang, China.

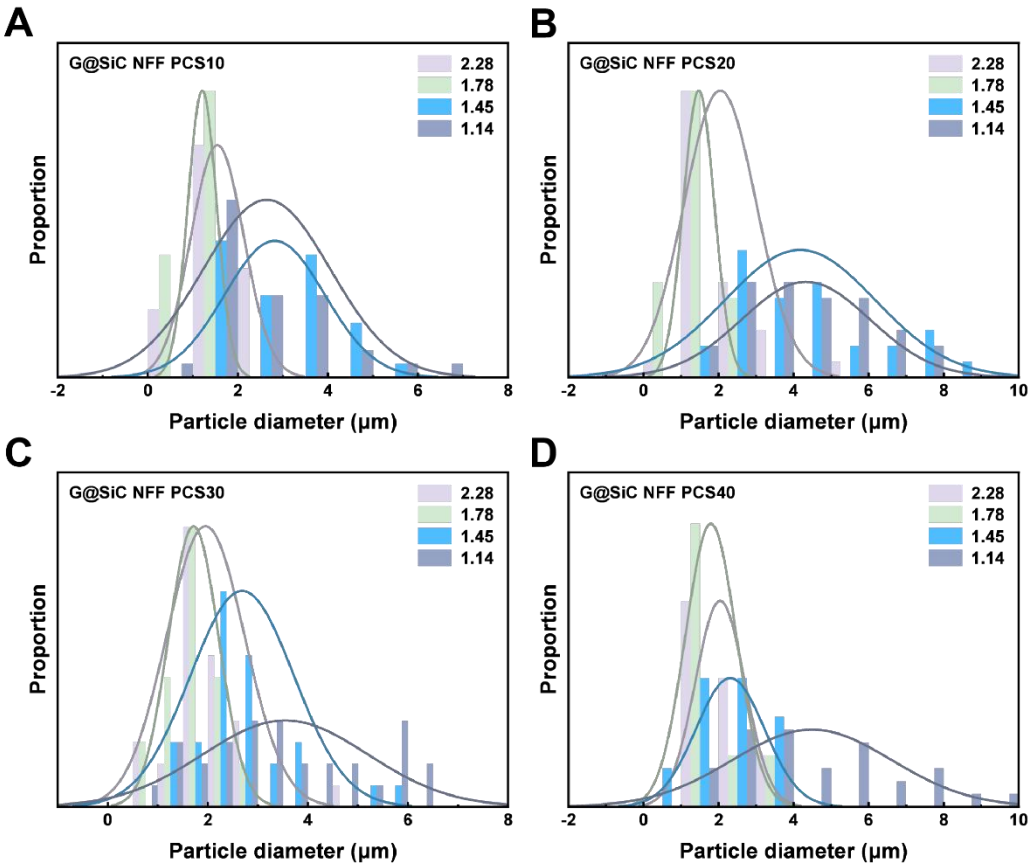
***Correspondence to:** Prof. Zheng Li, ZJU-Hangzhou Global Scientific and Technological Innovation Center, Key Laboratory for Biomedical Engineering of Education Ministry, Zhejiang Key Laboratory of Intelligent Sensing Technology and Advanced Medical Instrument, College of Biomedical Engineering & Instrument Science, Zhejiang University, Hangzhou 310027, Zhejiang, China. E-mail: li.zheng@zju.edu.cn; Prof. Xinxin Jin, Shao Xing Institute of Technology, School of Pharmacy and Health Sciences, Shaoxing Institute of Technology, Shaoxing 312000, Zhejiang, China. E-mail: jinxinxin@zsit.edu.cn; Dr. Yi Han, Hangzhou Gaoxi Technology Co., Ltd, Hangzhou 311113, Zhejiang, China. E-mail: firehuo@aliyun.com



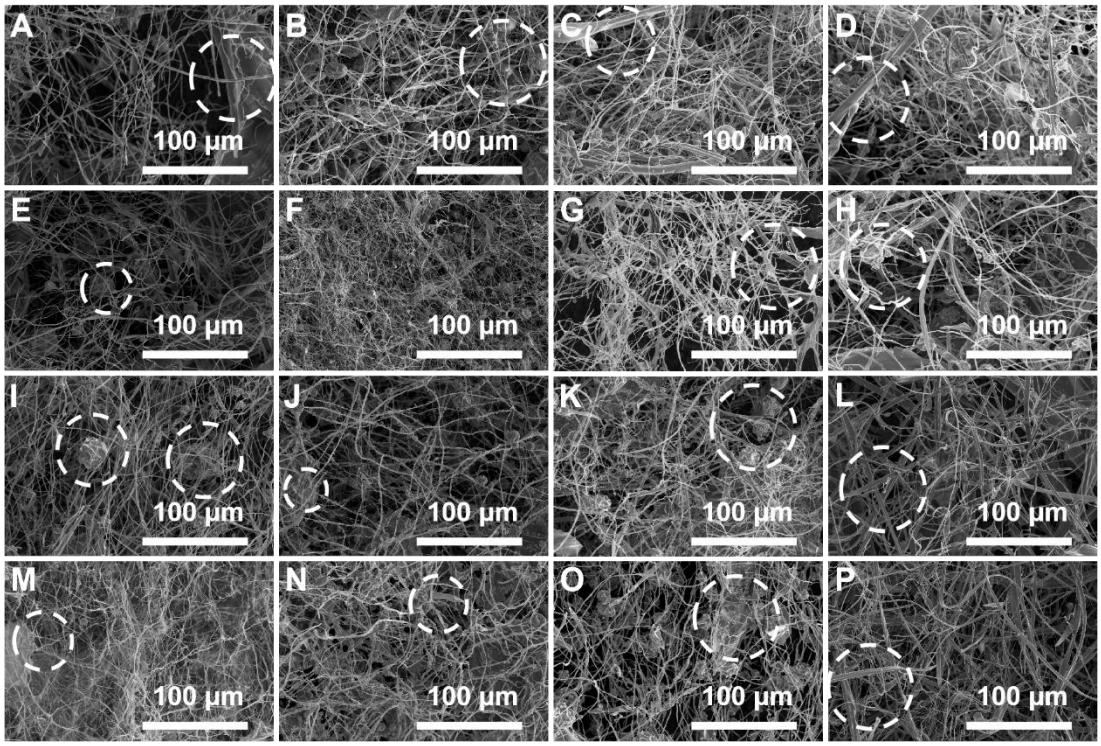
Supplementary Figure 1. Frequency-dependent viscoelastic properties of GO and PVP spinning solutions. Storage modulus (G′) and loss modulus (G″) as functions of angular frequency for spinning solutions with different PVP concentrations: (A) PVP2, (B) PVP4, (C) PVP6, and (D) PVP8. The rheological measurements were used to assess the viscoelastic compatibility of the GO core and PVP shell solutions for coaxial electrospinning.



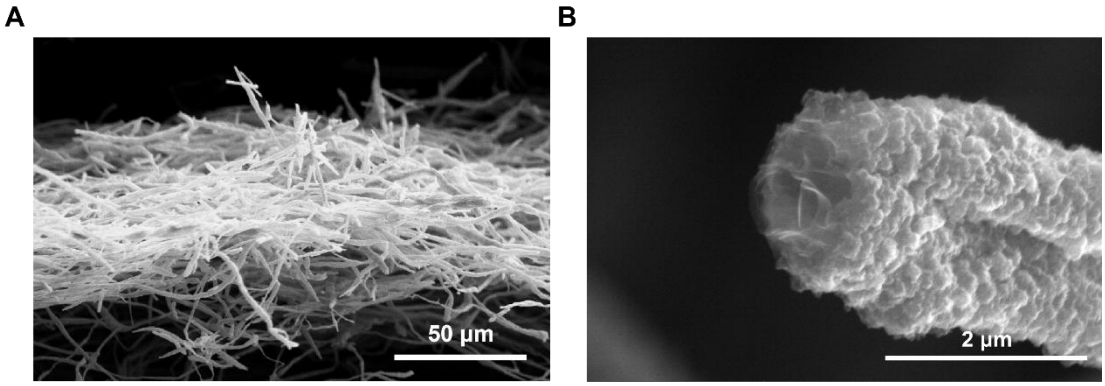
Supplementary Figure 2. Extensional behavior of inner and outer spinning solutions. Representative optical images showing liquid-bridge stretching and filament formation of the inner and outer spinning solutions, indicating their solution spinnability.



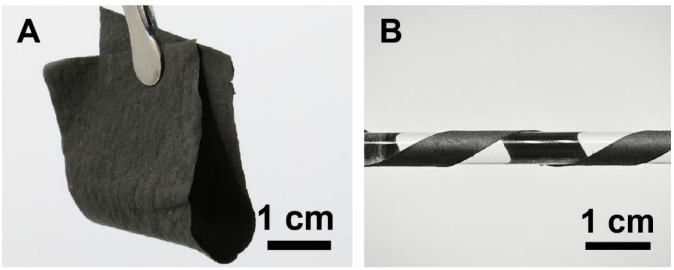
Supplementary Figure 3. Fiber diameter distributions under different PCS concentrations and shell-to-core flow rate ratios. (A-D) Histograms and fitted distribution curves showing the fiber diameter distribution of G@SiC precursor fibers prepared with PCS concentrations of 10, 20, 30, and 40 wt% at shell-to-core flow rate ratios of 2.28, 1.78, 1.45, and 1.14, respectively.



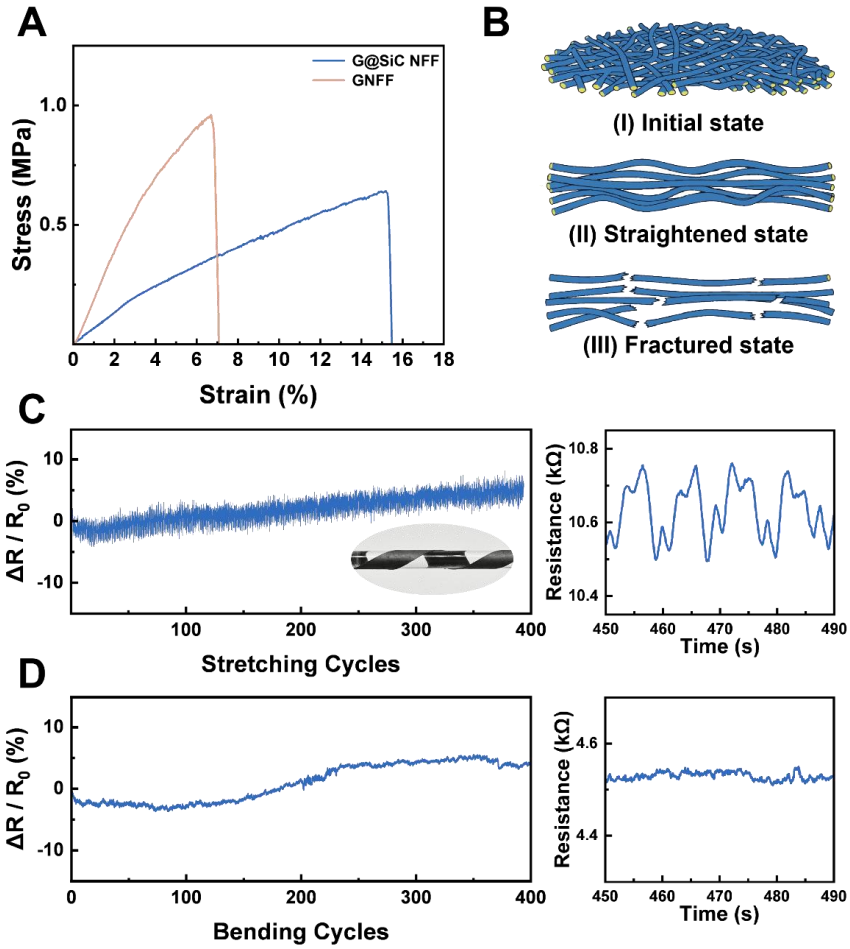
Supplementary Figure 4. Low-magnification SEM images of samples prepared with different PCS concentrations and shell-to-core flow rate ratios. The shell solution feed rate was fixed at 0.032 mL min^{-1}. The shell-to-core flow rate ratios for (A-D), (E-H), (I-L), and (M-P) were 2.28, 1.78, 1.45, and 1.14, respectively. Within each group, the PCS concentrations were 10, 20, 30, and 40 wt%, respectively. Dashed circles indicate representative regions where droplet-like defects or local fibre thickening are observed.



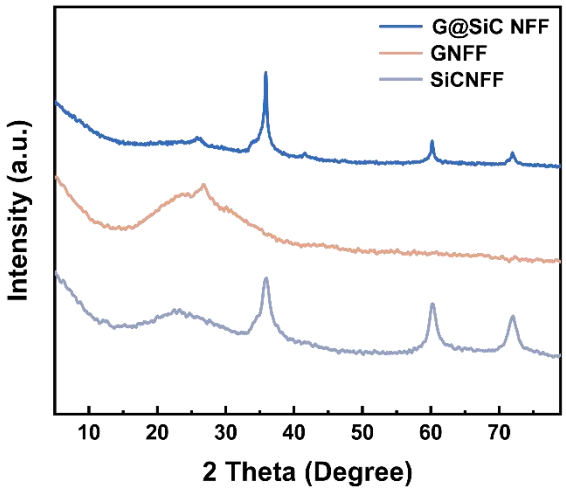
Supplementary Figure 5. Cross-sectional SEM images of G@SiC NFF. (A) Fibrous network. (B) Cross-sectional SEM image of an individual fiber.



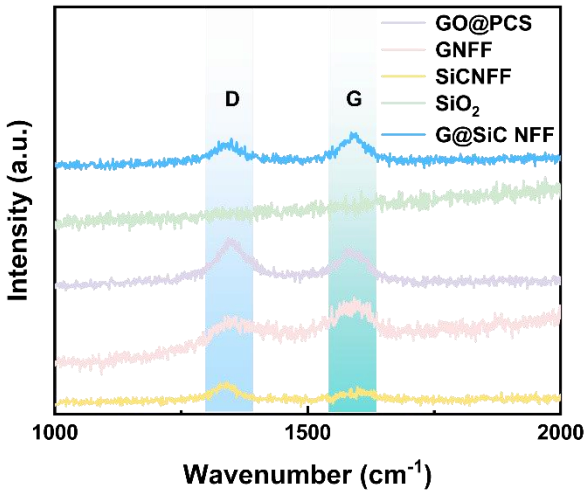
Supplementary Figure 6. Digital photographs showing (A) bent and (B) curled states of the G@SiC NFF.



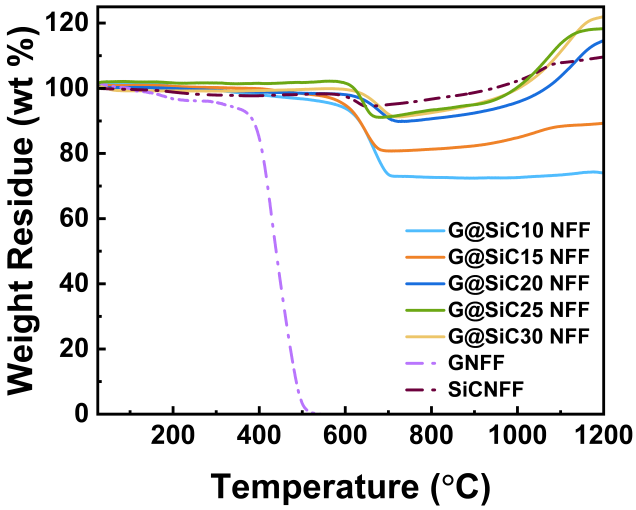
Supplementary Figure 7. Mechanical flexibility and electromechanical response of the freestanding G@SiC NFF. (A) Tensile stress-strain curves of G@SiC NFF and GNFF. (B) Schematic illustration of the fibrous network evolution during tensile deformation, showing the transition from a relaxed network to fiber alignment and fracture. (C, D) Relative resistance responses of G@SiC NFF during cyclic stretching and bending, respectively. The reversible resistance variation under repeated deformation indicate the mechanical compliance of the fabric and the preservation of conductive pathways. The bending test was performed at a bending radius of 2.5 mm.



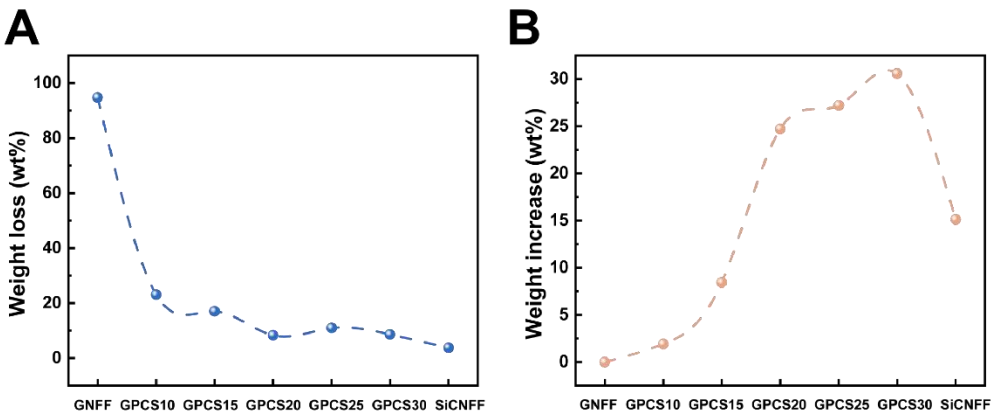
Supplementary Figure 8. XRD patterns of G@SiC NFF, GNFF, and SiC. The characteristic diffraction peaks confirm the coexistence of graphitic carbon and crystalline SiCNFF in the G@SiC NFF.



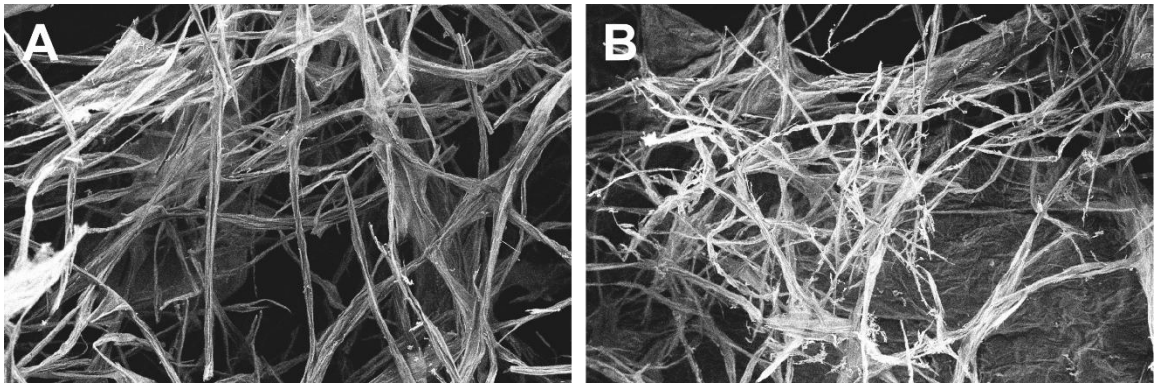
Supplementary Figure 9. Comparative Raman spectra of GNFF, GO@PCS, G@SiC NFF, SiCNFF, and SiO_2.



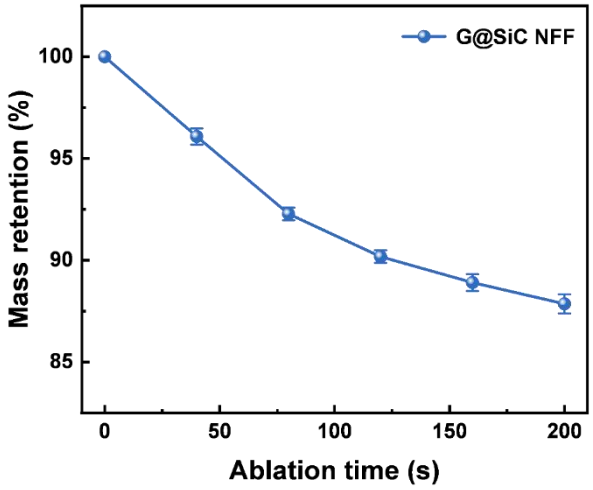
Supplementary Figure 10. PCS-concentration-dependent TGA curves of G@SiC NFFs in air, showing the effect of ceramic-shell formation on oxidative mass retention.



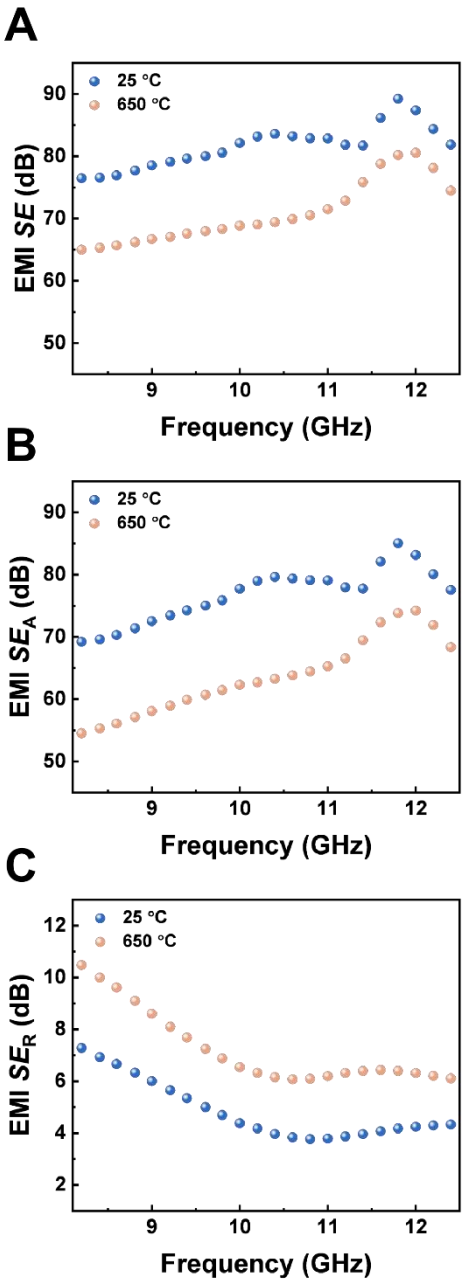
Supplementary Figure 11. Comparison of key parameters extracted from the TGA curves of G@SiC NFFs with different PCS contents in air: initial mass loss and high-temperature mass gain. GPCS10, GPCS15, GPCS20, GPCS25, and GPCS30 denote samples prepared with PCS contents of 10, 15, 20, 25, and 30 wt%, respectively, in the shell-forming formulation.



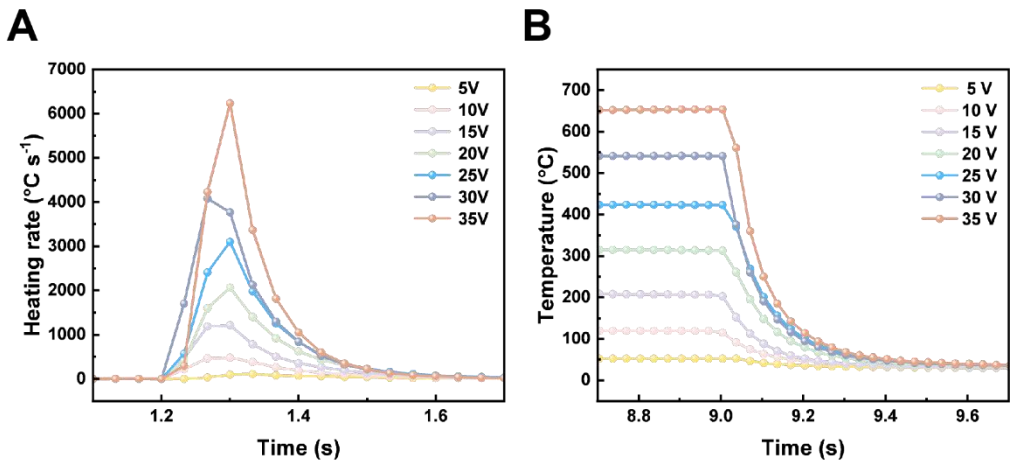
Supplementary Figure 12. SEM micrographs of G@SiC NFFs (A) before and (B) after alcohol-torch ablation at ~1100 °C for 180 s.



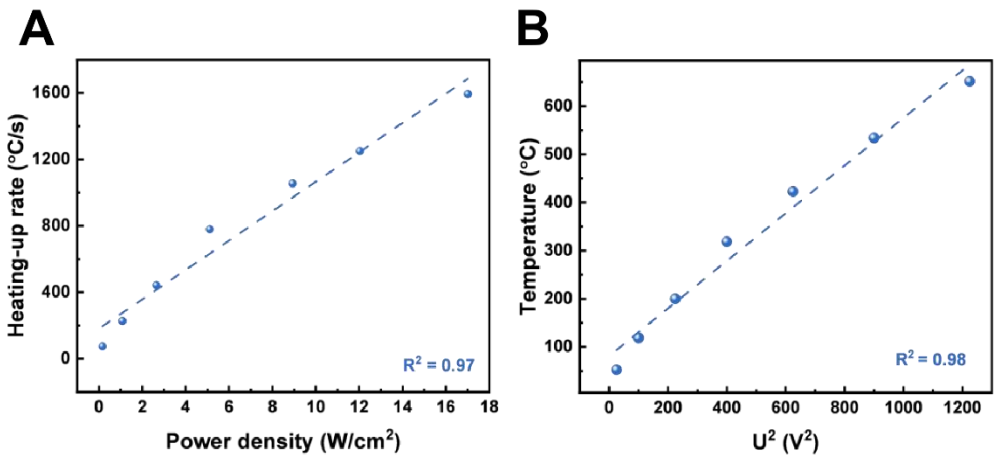
Supplementary Figure 13. Mass retention of G@SiC NFFs as a function of alcohol-torch exposure duration (0-200 s) at ~1100 ℃.



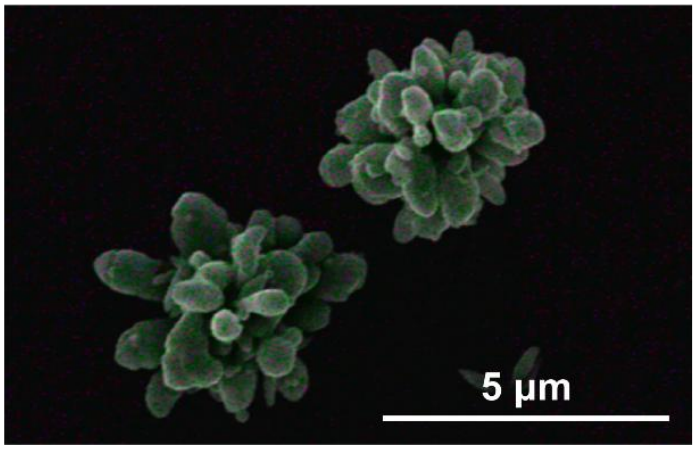
Supplementary Figure 14. Frequency-resolved EMI shielding components of G@SiC NFFs after isothermal oxidation in air at 650 °C. (A) Absorption shielding effectiveness (SE_A). (B) Reflection shielding effectiveness (SE_R). (C) Total shielding effectiveness (SE_T). All measurements were conducted in the X-band. The pristine sample measured at 25 °C was used as the reference.



Supplementary Figure 15. Transient heating and cooling kinetics of the G@SiC NFF. (A) Heating-rate profiles under different applied voltages; (B) Enlarged cooling profiles under different applied voltages.



Supplementary Figure 16. Scaling relationships of the Joule-heating behavior of the G@SiC NFF. (A) Heating rate as a function of power density; (B) Steady-state temperature as a function of the square of applied voltage.



Supplementary Figure 17. SEM image and corresponding EDS elemental maps.

Supplementary Movie 1: 120 min flame-tolerant electrical transport

Supplementary Movie 2: LED-circuit demonstration

Supplementary Movie 3: 1100 °C alcohol-torch ablation

Supplementary Table 1. Comparison of EMI shielding performance, thickness-normalized shielding effectiveness, and thermal stability of representative EMI shielding materials

Material	Thickness (mm)	EMI *SE* (dB)	*SE*/*t* (dB mm^{-1})	Frequency range (GHz)	Temperature (°C)	Ref.
Zn@$Ti_3C_2T_x$ MXene/CNF film	0.012	60.3	5025	8.2-12.4	25	[1]
Multilayered MXene/CNT film	0.036	81.4	2261.1	8.2-26.5	300	[2]
ANF@MXene fiber textile	0.213	83.4	391.5	8.2-12.4	300	[3]
MCC/MXene-POSS film	0.919	56.62	61.6	8.2-26.5	100	[4]
LCP/CNT segregated composite	2.0	39.8	19.9	8.2-12.4	200	[5]
PLLA/PDLA/CNT composite	3.0	44.1	14.7	8.2-12.4	180	[6]
PAEK-CNT/PEEK foam	0.8	18	22.6	8.2-40	315	[7]
PI/MXene/CF network	1.7	63.3	37.2	8.2-12.4	400	[8]
Graphene/SiC carbon cloth	0.45	74.2	164.9	8.2-12.4	380.2	[9]
ZrB_2/Al_2O_3 ceramic	1.2	44	36.6	8.2-12.4	600	[10]
ZrC/SiC nanofiber mat	1.8	20.1	11.2	8.2-12.4	600	[11]
Porous Ti_3SiC_2 ceramic	4.0	31.33	7.83	8.2-12.4	700	[12]
GNS/SiBCN nanocomposite	2	18	9	8.2-12.4	900	[13]
EVA/GP/MP/OMMT/SCF-derived ceramic	2.6	30	11.54	8.2-12.4	1000	[14]
G@SiC NFFs	0.08	76.7	958.76	8.2-12.4	650	This work

Supplementary Table 2. Quantitative elemental composition determined by EDS

Element	Wt%	At%
O	35.56	76.24
Zn	18.69	9.81
Ga	1.44	0.71
In	44.31	13.24
Total	100.00	100.00

REFERENCES

1. Da, Y.; Qu, Q.; Kong, L.; Liu, Q.; Zhu, M.; Du, Y.; Tian, X.; Liu, Y.; Wang, H. A high-performance, oxidation resistance and flexible Zn@MXene/cellulose nanofibers electromagnetic shielding film. *RSC Adv*. **2023**, *13*, 6619-6629. DOI: https://dx.doi.org/10.1039/d2ra07791d.

2. Shen, Y.; Yue, Y.; Li, H.; Li, Y.; Liu, H.; Zhou, B.; Feng, Y.; Liu, C.; Shen, C. Robust alternating multilayered MXene/CNT films for high-performance EMI shielding and Joule heating with superior fire/oxidation resistance. *Sci. China Mater*. **2025**, *68*, 4144-4154. DOI: https://dx.doi.org/10.1007/s40843-025-3578-5.

3. Liu, L.-X.; Chen, W.; Zhang, H.-B.; Ye, L.; Wang, Z.; Zhang, Y.; Min, P.; Yu, Z.-Z. Super-tough and environmentally stable aramid. nanofiber@MXene coaxial fibers with outstanding electromagnetic interference shielding efficiency. *Nano-Micro Lett*. **2022**, *14*, 111. DOI: https://dx.doi.org/10.1007/s40820-022-00853-1.

4. Si, Z.; Yan, Y.; Liu, X.; Xu, L.; Liao, H.; Nie, Z.; Xue, C.; Wan, G.; Wang, G. Flexible and multifunctional microcrystalline cellulose/$Ti_3C_2T_x$ MXene-POSS composite films for electromagnetic interference shielding in extreme environments. *Chem. Eng. J*. **2025**, *525*, 169897. DOI: https://dx.doi.org/10.1016/j.cej.2025.169897.

5. Liu, S.; Zhan, Y.; Sun, J.; Sun, Y.; Wang, W.; Pan, N.; Meng, Y.; Xia, H.; Jiang, X. High-temperature stable liquid crystalline polymer/carbon nanotube composites with a “brick-mortar” segregated structure for electromagnetic interference shielding. *Compos. Commun*. **2026**, *62*, 102720. DOI: https://dx.doi.org/10.1016/j.coco.2026.102720.

6. Liu, T.; Zhou, R.; Fei, Y.; Chen, F.; Liu, D.; Han, L.; Zhou, B.; Yang, J.; Kuang, T. Spatially directed carbon nanotube enrichment via polylactide stereocomplex formation enables exceptional thermal stability, high thermal conductivity, and electromagnetic interference shielding. *Compos. Commun*. **2025,** *60*, 102627. DOI: https://dx.doi.org/10.1016/j.coco.2025.102627.

7. Mei, X.; Wu, T.; Liang, L.; Bai, Y.; Jiao, J.; Guo, C.; Yang, Y.; Wang, G.; Zhang, S. Poly aryletherketone chemically modified multi-walled carbon nanotubes/poly etheretherketone electromagnetic interference shielding foam suitable for high temperature and strong corrosive media. *Mater. Today Nano* **2024**, *28*, 100538. DOI: https://dx.doi.org/10.1016/j.mtnano.2024.100538.

8. Wang, N.; Li, X.; Cao, W.; Yang, X.; Zou, X.; Fang, Y.; Shen, X.; Li, Q.; Song, N.; Xu, T.; et al. Lightweight polyimide nanocomposites with 3D cocarbonized

MXene/carbon fiber networks for electromagnetic interference shielding and high-temperature stability. *ACS Appl. Nano Mater*. **2025**, *8*, 7347-7359. DOI: https://dx.doi.org/10.1021/acsanm.5c00922.

9. Xu, Q.; Wang, C.; Hu, J.; Lu, P.; Wu, H.; Guo, B.; Tu, R.; Liu, K.; Yang, M.; Zhang, S.; et al. Graphene/SiC-coated textiles with excellent electromagnetic interference shielding, Joule heating, high-temperature resistance, and pressure-sensing performances. *J. Adv. Ceram*. **2023**, *12*, 778-791. DOI: https://dx.doi.org/10.26599/jac.2023.9220719.

10. Qing, Y.; Yao, H.; Li, Y.; Luo, F. Plasma-sprayed ZrB2/Al2O3 ceramics with excellent high temperature electromagnetic interference shielding properties. *J. Eur. Ceram. Soc*. **2021**, *41*, 1071-1075. DOI: https://dx.doi.org/10.1016/j.jeurceramsoc.2020.10.031.

11. Hou, Y.; Cheng, L.; Zhang, Y.; Du, X.; Zhao, Y.; Yang, Z. High temperature electromagnetic interference shielding of lightweight and flexible ZrC/SiC nanofiber mats. *Chem. Eng. J*. **2021**, *404*, 126521. DOI: https://dx.doi.org/10.1016/j.cej.2020.126521.

12. Yang, F.; Yao, J.; Du, W.; Huyan, W.; Peng, G.; Zhou, J.; Yao, Z. Ice-templated assembly strategy to construct oriented porous Ti_3SiC_2 ceramics for thermal management and electromagnetic interference shielding in harsh thermal environments. *J. Eur. Ceram. Soc*. **2023**, *43*, 3112-3121. DOI: https://dx.doi.org/10.1016/j.jeurceramsoc.2023.01.064.

13. Zhu, W.; Xia, X.; Zheng, Y.; Ji, H.; Su, D. Tailoring of carbon structure in lightweight GNS/SiBCN nanocomposites for enhanced electromagnetic interference shielding performance. *J. Eur. Ceram. Soc*. **2025**, *45*, 117180. DOI: https://dx.doi.org/10.1016/j.jeurceramsoc.2024.117180.

14. Li, Y.-M.; Deng, C.; Zhao, Z.-Y.; Han, L.-X.; Lu, P.; Wang, Y.-Z. Carbon fiber-based polymer composite via ceramization toward excellent electromagnetic interference shielding performance and high temperature resistance. *Compos. Part A Appl. Sci. Manuf*. **2020**, *131*, 105769. DOI: https://dx.doi.org/10.1016/j.compositesa.2020.105769.